Full Paper

INFLUENCE OF CALCINATION TEMPERATURE ON CIPROFLOXACIN PHOTODEGRADATION BY VANADIUM PENTOXIDE / GRAPHITIC CARBON NITRIDE PHOTOCATALYST

Khairunissa Syairah Ahmad Sohaimi[a,b] Juhana Jaafar[a]*

[a]Advanced Membrane Technology Research Centre (AMTEC), School of Chemical and Energy Engineering, Faculty of Engineering, Universiti Teknologi Malaysia, 81310 UTM Johor Bahru, Johor, Malaysia
[b]Faculty of Chemical Engineering Technology, Universiti Malaysia Perlis, 02100 Padang Besar, Perlis, Malaysia

*Corresponding author
juhana@petroleum.utm.my

Graphical abstract
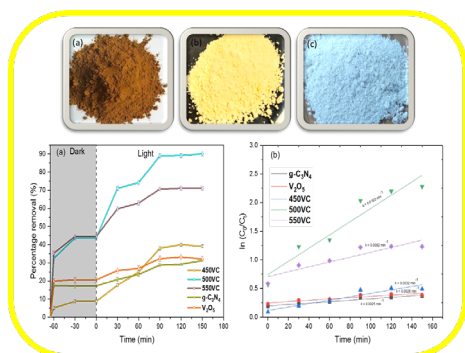
Abstract

The employment of vanadium pentoxide (V_2O_5) as a photocatalyst has been widely utilized owing to its promising supercapacitor properties for photocatalysis applications under visible light without any alteration. Up to date, there has yet to be a report on the investigation of calcination temperature effect on V_2O_5 and graphitic carbon nitride (g-C_3N_4) combination photocatalyst synthesis for ciprofloxacin (CIP) photodegradation. In this study, the V_2O_5 / g-C_3N_4 photocatalyst is synthesized using simple and facile calcination process. The properties of the synthesized V_2O_5 / g-C_3N_4 were evaluated in terms of porosity, surface morphology and composition elements, and its band gap value to well understand its' behaviour and interaction with CIP pollutants. The best synthesis conditions for V_2O_5 / g-C_3N_4 photocatalyst on CIP photocatalysis were at 500 °C (500VC) with 90.17 % CIP photodegradation performance. This research has provided a useful future reference in the field of photocatalysis research.

Keywords: Catalysts; Photocatalysis; Porous Materials; Pyrolysis; Ciprofloxacin.

1.0 INTRODUCTION

Endocrine-disrupting compounds (EDCs) like ciprofloxacin (CIP) are organic chemicals that have altered the endocrine system's activities and functions [1]–[3]. Human and animal infections are treated with fluoroquinolone antibiotic CIP. CIP can spread antibiotic-resistant bacteria and genes in aquatic ecosystems even at low concentrations. CIP is stable in water because it contains fluorine. Ozone and photocatalysis via advanced oxidation processes (AOPs) are widely used in the organic wastewater industry to address this issue [4], [5].

For energy conservation and environmental protection, finding photocatalysts with band gap energies that overlap visible light is the first task. V_2O_5, a 2D sheet material that can be used in visible light without alteration, has been intensively researched since 2011 [6], [7]. V_2O_5 nanostructures have a narrow band gap (2.3 eV), wide light

response, and stable chemical properties. V_2O_5's drawbacks include photo corrosion, electron-hole recombination, and low electronic conductivity [8]. Thus, V_2O_5 can be improved by attaching carbon nanostructures like activated carbon (AC) and graphitic carbon (GC). Graphite carbon nitride has high specific surface area, thermal and chemical stability, and an adequate energy band gap (2.7 eV). V_2O_5 and g-C_3N_4 can also form van der Waals heterojunctions [9].

The successful alignment of the conduction band (CB) (0.47 eV) and valence band (VB) (2.73 eV) of V_2O_5 with the CB (-1.2 eV) and VB (1.5 eV) of g-C_3N_4 led to the creation of photocatalyst heterojunctions have been reported [9],[10], [11]. Despite certain defects in the crystalline structure, this heterojunction enhances the efficiency of charge carrier separation, facilitates broad light-harvesting, and exhibits remarkable redox ability. Notably, the combination of V_2O_5 and g-C_3N_4 by calcination may affect their surface area and improve light absorption and charge separation and able to

degrade CIP pollutants effectively. Different photocatalysts had different best conditions with their targeted pollutants, so researchers have recently focused on the best condition calcination temperature. The surface's morphological and structural parameters show a variety of active response sites for the best photocatalysis process. Thus, the best V_2O_5 / g-C_3N_4 photocatalyst for CIP degradation for calcination temperature parameter in this study and their photocatalysis process mechanism remain unproven.

2.0 METHODOLOGY

2.1 Materials

Melamine and ammonium metavanadate (NH_4VO_3, Merck, USA) were utilized in the photocatalyst production. Sigma provided the CIP reference standard (United States). Merck provided sodium hydroxide and sulphuric acid for pH correction purposes (United States).

2.2 Synthesis of V_2O_5 / g-C_3N_4

To begin preparing g-C_3N_4, 15 g of melamine was added to a crucible, which was then covered with aluminium foil and heated in a muffle furnace at 550 °C for 2 hours at a heating rate of 2 °C / min [13]. Meanwhile, pure V_2O_5 was prepared by placing 5 g of NH_4VO_3 in a crucible and thermally treating it in a muffle furnace. For 1 hour, the thermal treatment was carried out at 550 °C at a heating rate of 5 °C/min [12]. About 20 mg of NH_4VO_3 was added to 1000 mg of g-C_3N_4 powder and ground together with an agate mortar for the synthesis of V_2O_5 / g-C_3N_4 photocatalyst. The ground powder was then placed in a covered crucible for calcination. The crucible was placed in a muffle furnace and heated for 3 hours at (450, 500 and 550 °C) at a rate of 5 °C/min.

2.3 Characterization of V_2O_5 / g-C_3N_4

Scanning electron microscopy (SEM, Hitachi SU8020) depict samples' surface shape and morphologies. Band gap studies were performed using LAMBDA 1050 UV-VIS/NIR spectrophotometer (UV-3600Plus, SHIMADZU). Meanwhile, X-ray Diffraction (XRD) was used to analyze the crystallinity of the photocatalyst using (XRD, Rigaku, SmartLab, USA). Lastly, the Brunauer-Emmett-Teller (BET) method (Thermo Scientific, USA) was employed to analyze the binary photocatalyst V_2O_5 / g-C_3N_4 with regards to its surface area, pore volume, and pore size characteristics.

2.4 CIP Photodegradation

Visible light photocatalytic activity of V_2O_5 / g-C_3N_4 was assessed by CIP reduction. About 0.1 g of the photocatalyst was placed in a 250 mL beaker containing 100 mL of CIP solution 10 ppm at pH 7. First, 60 min of the solution agitation were performed without light to determine the adsorption maximum time of CIP. Then, the mixture was irradiated by a 100 W LED (LED) for 150 min. The concentration of residual CIP was evaluated by UV-Vis Spectrophotometer at 277 nm after 30 minutes of sampling (Perkin Elmer, Lambda 25). The degradation performance in percentage (P) is estimated using the following Eq.1:

$$P = [(C_o - C_t) / C_o] \times 100\% \tag{1}$$

Whereby C_o and C_t are initial and final (at a specific time) concentrations of CIP, respectively.

3.0 RESULTS AND DISCUSSION

3.1 V_2O_5 / g-C_3N_4 Characterization

V_2O_5 / g-C_3N_4 was prepared by simple straightforward calcination process. Figure 1(a) and 1(b) illustrate the initial brownish appearance of V_2O_5 and the yellowish appearance of g-C_3N_4 prior to the calcination process. Following calcination at 500°C for 3 hours, the resulting product took on a slightly brownish-white material, as depicted in Figure 1(c), commonly referred to as 500VC. Following that, characterization analyses were performed. To determine a material's band gap, absorbance spectra were studied with Tauc plots for all samples of V_2O_5 / g-C_3N_4 with different calcination temperatures. As can be seen in Figure 2, the bandgap value of V_2O_5 and g-C_3N_4 alone were found to be 1.95 eV, and 2.71 eV which is consistent with the existing literature [14], [15]. The effects of V_2O_5 / g-C_3N_4 samples at different calcination temperatures of 450, 500 and 550 °C or known as 450VC, 500VC, and 550VC to band gap value are 2.78 eV, 2.64 eV and 2.0 eV respectively. This phenomenon showed that increasing of calcination temperature led to decreasing in band gap value. The calcination process can enhance the crystallinity of the photocatalyst. As the crystallinity improves, the energy levels of the valence and conduction bands become better defined, leading to a more accurate determination of the band gap [16]. Consequently, this refinement can lead to a decrease in the band gap value. After band gap values of all samples have been confirmed in visible light wavelength, the best V_2O_5 / g-C_3N_4 sample which was investigated through CIP degradation performance was taken for next analyses like SEM, XRD and BET together with pure V_2O_5 and g-C_3N_4. Based on CIP degradation performance, the best calcination temperature of V_2O_5 / g-C_3N_4 sample is 500 °C.

The SEM images in Figure 3(a)-(c) observed different of morphologies displayed. In Figure 3(a)-(b) showed the morphology of g-C_3N_4 and V_2O_5 respectively meanwhile Figure 3(c) showed 500VC images respectively. It can be seen that appearance of g-C_3N_4 and V_2O_5 in 500VC sample. According to the image of V_2O_5, it can be seen that irregular flake-shaped like structures [17] and meanwhile g-C_3N_4 showed as interconnected particles in bulk [13]. These two images of g-C_3N_4 and V_2O_5 showed in Figure 3(c) of 500VC sample shows the successful intercalation of these two materials by calcination process [18], [19]. In addition to morphological analyses of SEM, X-ray Diffraction can prove the successful formation of 500VC. In Figure 4(a), the XRD analysis reveals the presence of g-C_3N_4, characterized by two distinct peaks at 27.6°, indicative of (100) in-plane structural units, as illustrated in Figure 4(b) for g-C_3N_4 alone [20]. To confirm the presence of V_2O_5 in Figure 4(a), three

diffraction peaks at 20.3°, 26.1°, and 31.0° are identified, corresponding to the (001), (110), and (301) crystal planes of V_2O_5. These peaks align with the patterns observed in pure V_2O_5, as depicted in Figure 4(c) [21]. Notably, in Figure 4(a), the intensity of V_2O_5 peaks is relatively low, consistent with the quantities of V_2O_5 precursors compared to $g\text{-}C_3N_4$ during the sample synthesis. A similar pattern is observed when employing the same ratio of sample combination in XRD analysis, as reported in the literature [12]. As summarized in Table 1, the BET surface areas for V_2O_5, $g\text{-}C_3N_4$, 450VC, 500VC, and 550VC were measured at 4.77, 7.70, 16.34, 181.00, and 4.41 m^2/g, respectively. Notably, the combined material at 500 °C exhibited a surface area that was 25 times greater than that of $g\text{-}C_3N_4$ and V_2O_5 individually. This substantial surface area of 500VC played a pivotal role in the exceptional adsorption of CIP, attributed to the photocatalyst's surface properties and its efficient utilization of incident light during the photocatalytic degradation of CIP. As can be seen in Table 1, more increasing calcination temperature at 550 °C, the surface areas, pore volumes, and pore diameters decrease due to the crystallization of the $g\text{-}C_3N_4$ and V_2O_5 combination and part of pores have been blocked and led to decrease of surface area and porosity [20], [21]. Confirmation from XRD, BET and SEM analyses proved the successful incorporation between $g\text{-}C_3N_4$ and V_2O_5.

Figure 1. (a) V_2O_5 (b) $g\text{-}C_3N_4$ (c) 500VC photocatalyst samples.
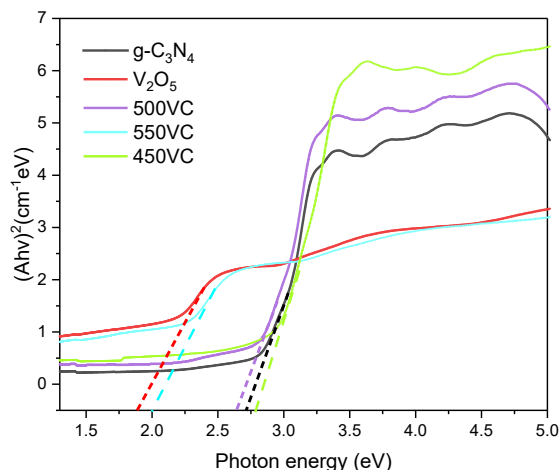

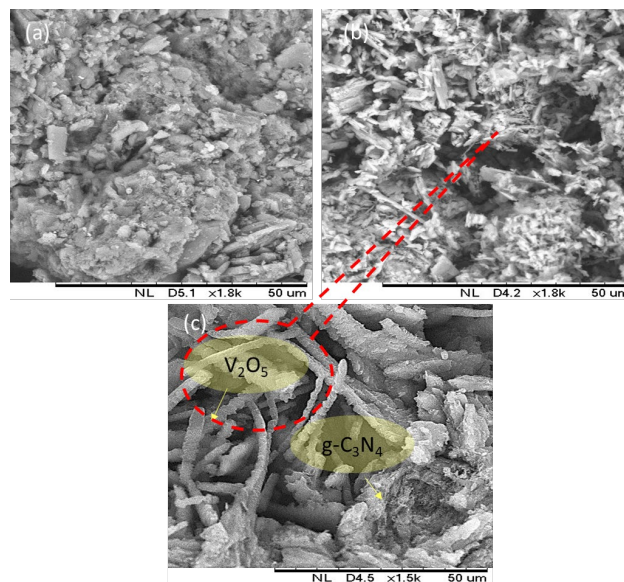**Figure 2.** Tauc's plot of V_2O_5 / $g\text{-}C_3N_4$ samples in different calcination temperatures.

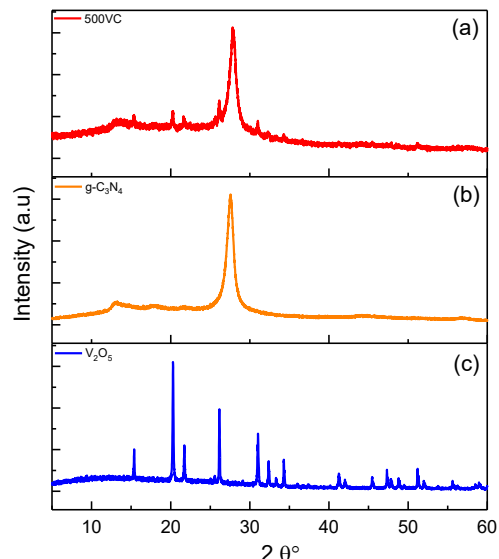**Figure 3.** SEM images of (a) $g\text{-}C_3N_4$ (b) V_2O_5 (c) 500VC samples respectively.

Figure 4. XRD analysis of (a) 500VC (b) $g\text{-}C_3N_4$ (c) V_2O_5

Table 1 BET surface area and pore structure of samples.

Samples	BET Surface Area (m^2/g)	Pore Volume (cm^3/g)	Average Pore Diameter (nm)
$g\text{-}C_3N_4$	7.70	0.059	30.76
V_2O_5	4.77	0.024	20.21
450VC	16.34	0.097	23.81
500VC	181.00	0.824	18.21
550VC	4.41	0.011	9.85

3.2 Effect of Calcination Temperature On The CIP Photocatalytic Activity by V_2O_5 / $g\text{-}C_3N_4$.

The photocatalytic activity of the photocatalysts was evaluated for the photodegradation of CIP under simulated sunlight. Without the presence of a catalyst, CIP did not degrade through photolysis under the simulated sunlight

conditions. To ensure adsorption equilibrium, the prepared samples were immersed in the CIP solution for 60 minutes in the absence of light. Figure 5(a) shows that all samples reached adsorption-desorption equilibrium within 45 to 60 minutes. Photoactivity of V_2O_5 / g-C_3N_4 was assessed by performing photodegradation of CIP under visible light for all the samples synthesized at 450, 500 and 550 °C or known as 450VC, 500VC and 550VC.

Interestingly, the calcination temperature affected photodegradation activity of V_2O_5 / g-C_3N_4 noticeably towards CIP solution as displayed in Figure 5(a). The photodegradation efficiencies of V_2O_5 / g-C_3N_4 prepared at 450, 500 and 550 °C were about 43.1 %, 90.17% and 71.7% for CIP solution, respectively. The V_2O_5 / g-C_3N_4 sample calcined at 500 °C displayed highest CIP photodegradation ability. It was analyzed that increasing calcination temperature from 450 °C to 500 °C led to increasing photodegradation efficiency and following that photocatalytic activity was found to follow a decreasing trend from 500 °C to 550 °C. The increased reaction rate of V_2O_5 / g-C_3N_4 calcined at 400 °C to 500 °C could be due to its higher heating temperature led to higher efficiency of absorbing visible light which can lead to better generation of photo-generated electrons causing more efficient separation of charge and hence better photoactivity [20]. Meanwhile, prolonged calcination at very high temperatures may lead to sintering, reduced surface area and decreased photodegradation efficiency like V_2O_5 / g-C_3N_4 at 550 °C [16]. When pollutants are present in a less concentrated form, we can assume a pseudo-first-order kinetics model as follows in Eq. (2):

$$Ln(C_0/C_t) = k_{app}t \qquad (2)$$

where k_{app} is the apparent rate constant (min^{-1}), and C_0 is the initial concentration of pollutants (mg L^{-1}) and C_t is the concentration of pollutants at time (mg L^{-1}). In the process of CIP photodegradation using the photocatalyst that was prepared, the kinetic parameter is assumed to be determined through a pseudo-first-order kinetic model. In this model, the rate constant k_{app} is determined as the slope of the fitted line depicted in Figure 5(b). The slope of the liner fitted graph shows the calculated k_{app} values of 0.0026, 0.0025, 0.0032, 0.0152, 0.0082 min^{-1} for V_2O_5, g-C_3N_4, 450VC, 500VC and 550VC respectively. Therefore, the outcome infers that the 500VC nanocomposite has had high reaction rate with 3.28 folds, compared with pure V_2O_5 and g-C_3N_4.
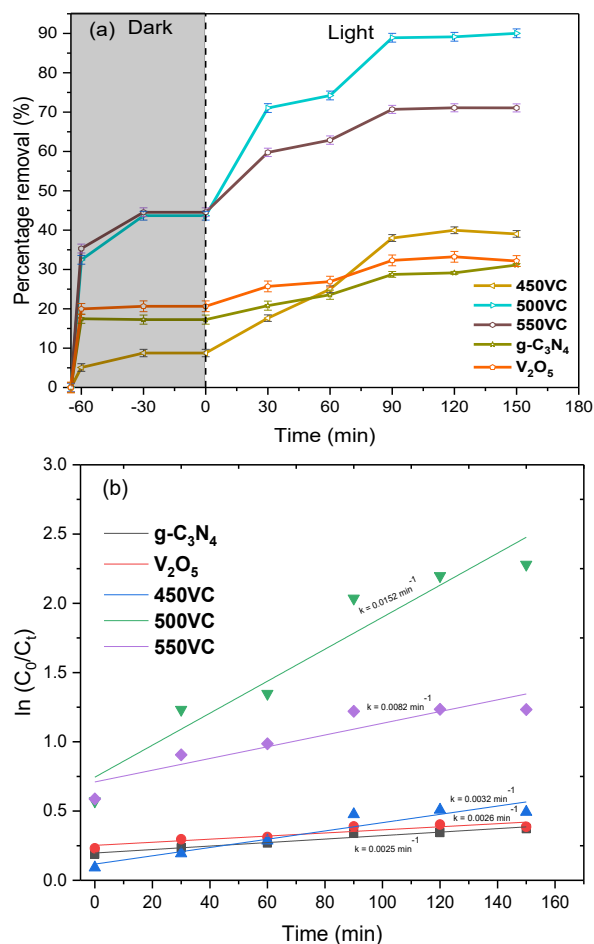

Figure 5. Photocatalytic activity of V_2O_5 / g-C_3N_4 for CIP photodegradation at (a) different calcination temperatures (b) kinetics CIP photodegradation with different calcination temperature of photocatalysts.

3.3 Radical Scavenger Studies

To elucidate the role of various reactive species (e$^-$, h$^+$, superoxide radicals (•O_2^-), and HO•) in the photodegradation of CIP, multiple quenching experiments were conducted under optimal conditions. In these experiments Silver nitrate (AgNO$_3$) and Ethylenediaminetetraacetic acid (EDTA) were used at a concentration of 1 mmol to scavenge e$^-$ and h$^+$, while Benzoquinone (BZQ) and butanol, also at the same concentrations, were employed to quench •O_2^- and HO• [12], [22]. The impact of each quenching agent on CIP photodegradation is illustrated in Figure 6. As anticipated, the results demonstrate varying degrees of reduction in CIP elimination efficiency in all cases, indicating the involvement of all the aforementioned reactive species in the photodecomposition process. The largest decrease in CIP photodegradation, amounting to 73.64 %, was observed in the presence of butanol, while the smallest decrease of 28.56 % was observed with BZQ. AgNO$_3$ and EDTA, the scavenger agents, reduced CIP photodecomposition by 45.77 % and 34.54 %, respectively. Consequently, •O_2^- species were found to contribute the most to CIP photodegradation, followed by positively charged holes (h$^+$)

in the second position. Negatively charged electrons (e^-) and HO• ranked third and fourth, respectively.
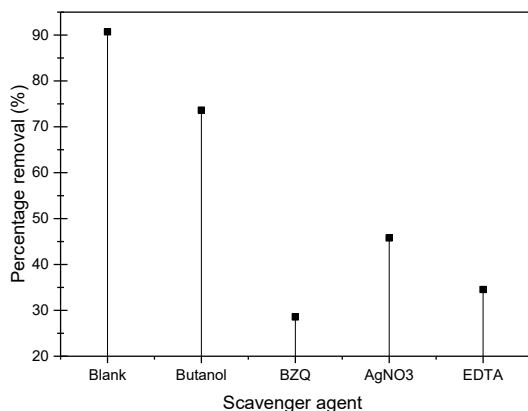

Figure 6. Photocatalytic degradation of CIP in the presence of different scavengers

4.0 CONCLUSION

In conclusion, the synthesis of V_2O_5 / g-C_3N_4 photocatalyst has been investigated with respect to the calcination temperature, aiming to enhance the photocatalytic degradation of ciprofloxacin antibiotics. Through systematic experimentation and analysis, it has been found that the highest performance in degrading ciprofloxacin, achieving approximately 90.17 % degradation, was achieved using a calcination temperature of 500 °C. The successful incorporation of V_2O_5 and g-C_3N_4, confirmed through XRD, SEM, and BET analyses, along with the band gap alteration, where surface area dominantly contributes to the highest photocatalytic degradation of ciprofloxacin. These findings not only advance our knowledge in the field of photocatalysis but also provide a solid foundation for future research in the development of efficient and sustainable photocatalytic systems for water treatment and environmental remediation.

Acknowledgement

Conflict of Interest

There are no conflicts present, as stated by the authors.

References

[1] A. Tarafdar *et al.* 2022. "The hazardous threat of Bisphenol A: Toxicity, detection and remediation," *Journal of Hazardous Materials*, 423: 127097. doi: 10.1016/j.jhazmat.2021.127097.

[2] J. Qiao and Y. Xiong. 2021. "Electrochemical oxidation technology: A review of its application in high-efficiency treatment of wastewater containing persistent organic pollutants," *Journal of Water Process Engineering,* 44: 102308. doi: 10.1016/j.jwpe.2021.102308.

[3] V. Vaezzadeh *et al.* 2021. "Examination of barnacles' potential to be used as bioindicators of persistent organic pollutants in coastal ecosystem: A Malaysia case study," *Chemosphere*, 263: 128272. doi: 10.1016/j.chemosphere.2020.128272.

[4] S. Kumar (S. Kumar), R. D. Kaushik, and L. P. Purohit. 2022. "ZnO-CdO nanocomposites incorporated with graphene oxide nanosheets for efficient photocatalytic degradation of bisphenol A, thymol blue and ciprofloxacin," *Journal of Hazardous Materials.* 424: 127332, 202. doi: 10.1016/j.jhazmat.2021.127332.

[5] R. Wang *et al.* 2023. "Cobalt-doped V2O5 hexagonal nanosheets for superior photocatalytic toxic pollutants degradation, Cr (VI) reduction, and photoelectrochemical water oxidation performance," *Environmental Resources,* 217: 114923. doi: 10.1016/j.envres.2022.114923.

[6] L. Parashuram *et al.* 2022. "Nitrogen doped carbon spheres from Tamarindus indica shell decorated with vanadium pentoxide; photoelectrochemical water splitting, photochemical hydrogen evolution & degradation of Bisphenol A," *Chemosphere*, 287: 132348. doi: 10.1016/j.chemosphere.2021.132348.

[7] H. Chaudhary *et al.* 2021. "Fabrication of reduced Graphene Oxide supported Gd3+ doped V2O5 nanorod arrays for superior photocatalytic and antibacterial activities," *Ceramic International*, 47: 32521–32533. doi: 10.1016/j.ceramint.2021.08.146.

[8] S. Sekar *et al.* 2021. "Graphitic carbon-encapsulated V2O5 nanocomposites as a superb photocatalyst for crystal violet degradation," *Environmental Resources,* 112201. doi: 10.1016/j.envres.2021.112201.

[9] X. Zhang *et al.* 2021. "V2O5/P-g-C3N4 Z-scheme enhanced heterogeneous photocatalytic removal of methyl orange from water under visible light irradiation," *Colloids and Surfaces A Physicochemical Engineering Aspects,* 608: 125580. doi: 10.1016/j.colsurfa.2020.125580.

[10] N. Ding *et al.* 2022. "Fluorinated inverse opal carbon nitride combined with vanadium pentoxide as a Z-scheme photocatalyst with enhanced photocatalytic activity," *Chinese Chemical Letter*, vol. 33: no. 8, pp. 3797–3801. doi: 10.1016/j.cclet.2021.11.042.

[11] J. Liu, X. Wei, W. Sun, X. Guan, X. Zheng, and J. Li. 2021. "Fabrication of S-scheme CdS-g-C3N4-graphene aerogel heterojunction for enhanced visible light driven photocatalysis," *Environmental Resources*, 197: 111136. doi: 10.1016/j.envres.2021.111136.

[12] J. H. Shen, T. H. Chiang, C. K. Tsai, Z. W. Jiang, and J. J. Horng. 2022. "Mechanistic insights into hydroxyl radical formation of Cu-doped ZnO/g-C3N4composite photocatalysis for enhanced degradation of ciprofloxacin under visible light: Efficiency, kinetics, products identification and toxicity evaluation," *Journal of Environmental Chemical Engineering*, 10: 107352. doi: 10.1016/j.jece.2022.107352.

[13] S. Le *et al.* 2021. "V2O5 nanodot-decorated laminar C3N4 for sustainable photodegradation of amoxicillin under solar light," *Applied Catalysis B Environmental*, 303: 120903. doi: 10.1016/j.apcatb.2021.120903.

[14] T. Xie *et al.* 2019. "Synthesis of multifunctional photocatalyst vanadium oxide/activated carbon via in situ utilization of stone coal ore," *Ceramic International*, 45: 4934–4944. doi: 10.1016/j.ceramint.2018.11.193.

[15] N. Q. Thang *et al.* 2021. "Localized surface plasmonic resonance role of silver nanoparticles in the enhancement of long-chain hydrocarbons of the CO2 reduction over Ag-gC3N4/ZnO nanorods photocatalysts," *Chemical Engineering.*

Science, 229: 116049. doi: 10.1016/j.ces.2020.116049.

[16] S. Phromma, T. Wutikhun, P. Kasamechonchung, T. Eksangsri, and C. Sapcharoenkun. 2020. "Effect of calcination temperature on photocatalytic activity of synthesized TiO2 nanoparticles via wet ball milling sol-gel method," *Applied Sciences*, 10: no. 3. doi: 10.3390/app10030993.

[17] A. A. Yadav, Y. M. Hunge, S. W. Kang, A. Fujishima, and C. Terashima. 2023. "Enhanced Photocatalytic Degradation Activity Using the V2O5/RGO Composite," *Nanomaterials*, 13: pp. 1–10. doi: 10.3390/nano13020338.

[18] S. Vignesh *et al.* 2022. "Investigation of heterojunction between α-Fe2O3/V2O5 and g-C3N4 ternary nanocomposites for upgraded photo-degradation performance of mixed pollutants: Efficient dual Z-scheme mechanism," *Journal of Alloys Compound*, 902: 163705. doi: 10.1016/j.jallcom.2022.163705.

[19] Y. N. Zang *et al.* 2021. "A biochar-promoted V2O5/g-C3N4Z-Scheme heterostructure for enhanced simulated solar light-driven photocatalytic activity," Royal Science Chemistry Advances, 11: 15106–15117. doi: 10.1039/d1ra02712c.

[20] M. G. Kim *et al.* 2021. "Effects of Calcination Temperature on the Phase Composition, Photocatalytic Degradation, and Virucidal Activities of TiO2Nanoparticles," *American Chemical Society Omega*, 6: 10668–10678. doi: 10.1021/acsomega.1c00043.

[21] L. Huang *et al.* 2018. "Influence of calcination temperature on the plate-type V2O5–MoO3/TiO2 catalyst for selective catalytic reduction of NO," *Reaction Kinetic Mechanism Catalysis,* 124: 603–617. doi: 10.1007/s11144-018-1378-0.

[22] K. Duan *et al.* 2022. "A facile route to synthesize n-SnO2/p-CuFe2O4 to rapidly degrade toxic methylene blue dye under natural sunlight," *Royal Science Chemistry Advances*, 12: 16544–16553. doi: 10.1039/d2ra01690g.